

1 **Chemogenetic activation of astrocytes in the hippocampus and cortex changes**
2 **the transcriptome of microglia and other cell types.**

3 Stéphanie Philtjens^{1,2#}, Marion T. Turnbull^{3,4#}, Brian P. Thedy³, Younghye Moon^{1,2}, Jungsu
4 Kim^{1,2*}

5

6 #Equal contribution

7 ¹Department of Medical and Molecular Genetics, Indiana University School of Medicine,
8 Indianapolis, IN 46202, USA

9 ²Stark Neuroscience Research Institute, Indiana University School of Medicine, Indianapolis, IN
10 46202, USA

11 ³Department of Neurology, Mayo Clinic, Jacksonville, FL 32224, USA

12 ⁴Department of Neuroscience, Mayo Clinic, Jacksonville, FL 32224, USA

13

14

15 *Corresponding author:

16 Jungsu Kim, Ph.D.

17 320 W. 15th Street, NB Bldg Rm 102A

18 Indianapolis, IN 46202

19 Phone: 317-278-6351

20 Fax: 317-274-0067

21 Email: jk123@iu.edu

22

23 Key words:

24 single cell RNA sequencing – DREADDS – astrocytes – microglia – chemogenetics

25 **Abstract**

26 Astrocytes are the most common glial cell type in the brain, yet, it is still not clear how their
27 activation affects the transcriptome of other brain cells such as microglia and neurons.
28 Engineered G protein-coupled receptors called Designer Receptors Exclusively Activated by
29 Designer Drugs (DREADDs) make it possible to selectively activate specific cell types, such as
30 neurons and astrocytes. By combining the selective activation of astrocytes with single cell RNA
31 sequencing, we were able to study transcriptional changes that occur in response to the
32 activation of astrocytes at the single cell level. Interestingly, our data shows that long-term
33 activation of astrocytes in healthy mice results in dramatic alteration in the transcriptome of
34 astrocytes and microglia. Genes that were differentially expressed in these Gq-DREADD-
35 activated astrocytes were involved in neurogenesis and low density lipoprotein particle biology,
36 while those in the microglia were involved in the response to lipoproteins, and the migration and
37 chemotaxis of immune cells. Furthermore, network analysis showed that Gq-DREADD-
38 mediated activation in astrocytes resulted in an upregulation of genes involved in the G protein-
39 coupled receptor signaling pathway and calcium ion homeostasis. This confirmed the activation
40 of astrocytes through the expressed DREADDs. Our findings show the importance of
41 considering the transcriptomic alteration in microglia and neurons after the activation of
42 astrocytes in *in vivo* models. Therefore, our data will serve as a resource for the broader
43 neuroscience community.

44 **Introduction**

45 Astrocytes are the most abundant glial cell in the brain and affect most aspects of neural
46 function. They are responsible for neurotransmitter and ion homeostasis at the level of the
47 synapse, provide trophic support to neurons, regulate blood flow, and provide energy substrates
48 (Abbott, Rönnbäck *et al.* 2006, Sofroniew and Vinters 2010). Correspondingly, in disease states,
49 astrocytes can undergo morphofunctional remodeling called 'reactive astrogliosis', where
50 normal homeostatic mechanisms are lost and pro-inflammatory responses are upregulated
51 (Ridet, Privat *et al.* 1997, Zamanian, Xu *et al.* 2012, Liddelow and Barres 2017). This reactive
52 phenotype may contribute to disease progression or may even trigger initial pathological
53 changes (Sofroniew and Vinters 2010). Thus a better understanding of how changes in
54 astrocyte function affects surrounding cells *in vivo* would be critical for our understanding of
55 normal physiology and disease progression.

56 To fully characterize the complex molecular interactions between astrocytes and
57 neighboring cells *in vivo*, we used a combination of chemogenetics and single cell RNA
58 sequencing (scRNA seq). Expression of engineered G protein-coupled receptors (GPCR),
59 called Designer Receptors Exclusively Activated by Designer Drugs (DREADDs), in astrocytes
60 allows for activation of this cell type through selective binding of its ligand (Lee, Giguere *et al.*
61 2014, Urban and Roth 2015, Roth 2016). These mutated muscarinic receptors respond
62 exclusively to clozapine-N-oxide (CNO) and are unresponsive to their endogenous ligand
63 acetylcholine (Armbruster, Li *et al.* 2007, Rogan and Roth 2011). In this study we used the Gq-
64 coupled human muscarinic type 3 receptor (hM3Dq) whose activation results in Ca²⁺
65 mobilization and ERK1/2 phosphorylation (Armbruster, Li *et al.* 2007). The *in vivo* functionality of
66 DREADD-mediated astrocyte activation has previously been demonstrated in rats, with
67 excitation of hM3D-expressing astrocytes in the nucleus accumbens core resulting in glutamate
68 gliotransmission and modulated drug seeking behavior (Bull, Freitas *et al.* 2014, Scofield, Boger

69 et al. 2015). However the effect on astrocyte activation on surrounding cells was not
70 investigated.

71 Recent scRNA seq technologies have made it possible to study transcriptional
72 differences in each cell-type in healthy and diseased brains, as well as in brain injuries such as
73 traumatic brain injury (Keren-Shaul, Spinrad et al. 2017, Arneson, Zhang et al. 2018, Batiuk,
74 Martirosyan et al. 2020). In this study, we were interested in the transcriptional changes that
75 occur after astrocyte-specific activation using the Gq-DREADD. To selectively activate
76 astrocytes in our study, we used adeno-associated virus transduction of Gq-DREADD into the
77 hippocampus and cortex of wild type mice under the control of the glial fibrillary acidic promoter
78 (GFAP). We administered CNO to our mice over a two month period to simulate chronic
79 activation of astrocytes instead of initiating an acute injury response. We profiled a total of
80 34,736 cells and showed that Gq-DREADD activation in astrocytes does not only change the
81 transcriptional profile of the astrocytes themselves, but also of neighboring microglia. Network
82 analysis using MetaCore™ showed that the genes that were upregulated in the astrocytes after
83 CNO treatment activation were involved in GPCR signaling and calcium homeostasis, which
84 confirmed Gq-DREADD-mediated activation of astrocytes. No major transcriptional changes
85 were observed in the neurons or other cell types present in the brain such as endothelial and
86 ependymal cells. To the best of our knowledge, our study is the first to study the effect of
87 astrocyte-specific Gq-DREADD activation in surrounding brain cell types at the single cell level
88 using scRNA seq.

89 **Material and Methods**

90 ***Plasmid preparation and AAV packaging***

91 pAAV-GFAP-hM3D(Gq)-mCherry was a gift from Bryan Roth (plasmid # 50478;
92 <http://n2t.net/addgene:50478>; RRID:Addgene_50478). Plasmid DNA was prepared and purified
93 using a QIAGEN Plasmid Maxi Kit (Qiagen, Cat. No. 12163) per the manufacturer's protocol.
94 AAV particles were packaged into serotype 5 type capsid and purified using standard methods
95 (Zolotukhin, Byrne et al. 1999). Briefly, AAV was generated by co-transfection with the cis
96 plasmid pDP5 (Plasmid Factory, AAV5 helper plasmid) into HEK293T cells. Cells were
97 harvested 72 h after transfection, treated with 50 Units/ml Benzonase (Sigma Aldrich), and
98 lysed by freeze thaw. The virus was then purified using a discontinuous iodixanol gradient and
99 buffer exchanged to phosphate buffered saline (PBS) using an Amicon Ultra 100 Centrifugation
100 device (Millipore). The genomic titer of each virus was determined by quantitative PCR using
101 the ABI 7700 (Applied Biosystems) and primers specific to the WPRE. The viral DNA samples
102 were prepared for quantification by treating the virus with DNaseI (Invitrogen) and Proteinase K,
103 and samples were compared against a standard curve of supercoiled plasmid diluted to 1⁴ to 1⁷
104 copies per ml. AAV5 is astrocyte specific and its injection into the striatum and substantia nigra
105 has previously demonstrated astrocyte-specific expression with no expression in neurons or
106 microglia (Drinkut, Tereshchenko et al. 2012, Merienne, Le Douce et al. 2013).

107 ***Animals***

108 All experiments were approved by the Mayo Clinic Institutional Animal Care and Use Committee
109 (IACUC). Male C57BL6/6J mice (The Jackson Laboratory; stock number #000664) were group
110 housed and allowed to acclimate to their new environment for 1 week before surgery. Mice were
111 housed on a 12 hour dark/light cycle with water and standard chow available *ad libitum*.

112 **Stereotaxic Surgery**

113 8 week-old mice (19-24 g) were anesthetized by intraperitoneal (i.p.) injection of ketamine (100
114 mg/kg) and xylazine (10 mg/kg) and placed on a stereotaxic instrument. The skin was opened
115 and a hole in the skull was made by a hand held drill. The needle was lowered into the
116 hippocampus (A-P -2 mm; M-L \pm 1.5 mm; D-V -1.7 mm from Bregma) and the virus (AAV-GFAP-
117 hM3D(Gq)-mCherry; Serotype 5; 1.0×10^{12} genome copies/ml) was infused at a rate of 0.4 μ l/min
118 (1.5 μ l total volume). The needle was allowed to remain in place for 5 minutes then slowly raised
119 0.9 mm to the cortex (A-P -2 mm; M-L \pm 1.5 mm; D-V -0.8 mm from Bregma) and more virus was
120 infused (0.4 μ l/min; 1.0 μ l total volume). The needle was again left for 5 minutes before being
121 removed. This was repeated on the contralateral hemisphere for bilateral injection of the virus
122 into both hippocampi and cortex (Figure 1A).

123 **Chronic CNO Administration**

124 CNO (Hello Bio; Cat # HB1807) was dissolved in clean drinking water at 0.25 mg/ml to
125 approximate a 5mg/kg/day dose of CNO. 5 mM of saccharin (Sigma Aldrich, Cat. No. 109185)
126 was added to mask the bitter taste of CNO and control groups had only saccharin in their
127 drinking water. Mouse cage water containing CNO and saccharin was carefully monitored and
128 changed for fresh CNO/saccharin every two to three days. CNO/saccharin was given for two
129 months after stereotaxic surgery.

130 **Tissue Preparation and Immunohistochemistry**

131 For tissue that was to be assessed histologically, mice were sacrificed by ketamine (100mg/kg
132 i.p.) overdose followed by transcardial perfusion with 4% paraformaldehyde (PFA). Tissue was
133 post-fixed in 4% PFA overnight at 4°C, and then left for 24 h in PBS containing 30% sucrose.
134 Tissue was then embedded in Frozen Section Compound (FSC22; Leica) and sections were cut
135 in the coronal plane (30 μ m) using a cryostat.

136 Fluorescence immunohistochemistry was performed on free floating coronal sections to
137 identify mCherry-positive cells and GFAP-positive astrocytes in the hippocampus and cortex.
138 Briefly, sections were blocked for 1 h at room temperature in 5% bovine serum albumin (BSA),
139 and 0.1% Triton-X in PBS followed by incubation overnight in rabbit anti-GFAP antibody
140 (1:1000; Thermo Fisher Scientific, Cat. No. 2.2B10), and rabbit anti-mCherry (Abcam, Cat. No.
141 ab167453), mouse anti-NeuN (1:1000; Novus Cat. No. NBP1-92693) or rabbit anti-Iba1 (1:1000;
142 Wako Cat. No. 019-19741). After washing in 0.1% Triton-X in PBS, sections were incubated in
143 AlexaFluor 488, 594 and 647 (1:1000; Invitrogen) and DAPI (1:1000; Thermo Scientific) for 2 h.
144 Sections were then washed and coverslipped with Prolong Antifade Diamond Mountant
145 (Invitrogen). Fluorescence microscopy was performed using a fluorescence slide scanner
146 (Aperio, Leica Biosystems).

147 **Isolation of cells**

148 Mice were sacrificed by ketamine (90mg/kg i.p.) and xylazine (10 mg/kg) overdose followed by
149 transcardial perfusion with ice cold PBS (approx. 20 ml). Hippocampal and cortical tissue
150 containing the virus was dissected out from the freshly isolated brain. The tissue was minced
151 with a razor blade and incubated for 30 min in ice-cold accutase (StemPro Accutase, Fisher
152 Scientific, Cat. No.: A1110501) at 4°C. The dissociated tissue was centrifuged at 300g for 10
153 min at 4°C. The pellet was resuspended in ice-cold Hanks' Balanced Salt solution (Life
154 Technologies, Cat. No.: 14025-092) and triturated with a 15 mL serological pipette. This step
155 was repeated until the entire tissue was dissociated. Next, the sample was filtered first through

156 a 70 μ m cell strainer, followed by a 40 μ m cell strainer. The cells were centrifuged at 300g for 5
157 min at 4°C.

158 ***Myelin removal***

159 Myelin removal was performed following the Miltenyi's Myelin Depletion Protocol. In short, the
160 pellet obtained during cell isolation was resuspended in magnetic-activated cell sorting (MACS)
161 buffer (PBS + 0.5% BSA (ThermoFisher, Cat. No.: AM2618)), myelin removal beads (Miltenyi
162 Biotec, Cat. No.: 130-096-733) were added, and the solution was incubated for 15 min at 4°C.
163 The cells were centrifuged at 300g for 10 min at 4°C, the pellet was resuspended in MACS
164 buffer and the solution was passed through LS columns (Miltenyi Biotec, Cat. No.: 130-042-
165 401). The cells were centrifuged at 300g for 15 min at 4°C, the pellet was resuspended in
166 MACS buffer, centrifuged again at 300g for 15 min at 4°C and resuspended in PBS containing
167 0.01% BSA.

168 ***Single cell RNA sequencing***

169 The obtained single cells were subjected to droplet-based single cell RNA sequencing. The 10x
170 Genomics Chromium™ Single Cell 3' Library & Gel Bead Kit v2 was used per manufacturer's
171 instructions. The libraries were sequenced on an Illumina NovaSeq 6000 SP at the Indiana
172 University Center of Medical Genomics. The 10x Genomics software Cell Ranger v.3.0.2 was
173 used for sample demultiplexing, barcode processing and single cell counting. All samples were
174 aligned against the mouse reference genome (mm10).

175 Subsequent data analysis was performed using the R (v.3.5.2) package Seurat v.3.0.2
176 (Butler, Hoffman et al. 2018, Stuart, Butler et al. 2019). Standard quality control included the
177 removal of cells with a mitochondrial count >5%, as well as cells with less than 200 and more
178 than 2,000 detected genes. A total of 34,736 cells remained after quality control filtering steps.
179 The data were log-normalized using a scaling factor of 10,000, scaled and regressed against
180 the percentage of mitochondrial content. Principal component analysis (PCA) was performed
181 with the top 3,000 most variable genes and the number of PCAs to use were determined after
182 1,000 permutations using the ElbowPlot. The first 21 PCAs was used to determine the K-
183 nearest neighbor (KNN) and cluster the cells into 15 different cell clusters. The clustering
184 resolution used was 0.5. Marker genes for naming the clusters were determined using the
185 FindConservedMarkers function in Seurat. Cells from the glial and neuronal clusters (astrocytes,
186 microglia I-V, mixed glia I, mixed glia II, neurons) were taken for re-clustering.

187 ***Analysis of differential gene expression***

188 Differential gene expression analysis between the control group (saccharin) and the Gq-
189 DREADD group (CNO) was done in Seurat using a likelihood test assuming an underlying
190 negative binomial distribution. Genes with a p-value < 0.05 after Bonferroni correction were
191 considered to be significantly differentially expressed between both groups. The differentially
192 expressed genes were analyzed for functional enrichment using g:Profiler (Raudvere, Kolberg
193 et al. 2019), and network analysis was performed using the Analyze Networks algorithm in
194 MetaCore™ (Clarivate Analytics, v.19.4 build 69900).

195 **Results**

196 ***Astrocyte-Specific Expression of Gq-DREADD***

197 Microinjection of AAV5-GFAP-hM3D(Gq) resulted in virus spread around the hippocampal and
198 cortical injection points. Histological visualization with the fluorescent reporter mCherry

199 confirmed that Gq-DREADD expression remained restricted to astrocytes based on their co-
200 localization with the astrocyte marker GFAP (Figure 1B and 1C) and morphology consistent with
201 astrocytic immunoreactivity patterns (Bushong, Martone *et al.* 2002, Benediktsson, Schachtele
202 *et al.* 2005, Scofield, Boger *et al.* 2015). Moreover, mCherry did not show co-localization with
203 the neuronal marker, NeuN, or the microglial marker, Iba1 (Supplementary Figure 1A & 1B).

204 ***Single cell RNA sequencing identifies fifteen different cell types***

205 To determine how activation of astrocytes affects the transcriptome of astrocytes and other cell
206 types, we performed scRNA seq on cells isolated from the hippocampus and cortex of four
207 month-old C57BL/6J mice. These mice were injected with AAV-GFAP-hM3D(Gq) at 8 weeks of
208 age (Figure 1A) and treated with CNO or saccharin for 8 weeks. Two samples per group were
209 sequenced with an average of 442M reads per sample, or an average of 37,000 reads per cell.
210 About 56% of all reads were exonic, while 29% were intronic and only 5% were intergenic. A
211 total of 34,736 cells passed the quality control filters, 16,107 cells in the CNO treated group and
212 18,629 cells in the negative control group (saccharin). Unsupervised clustering resulted in the
213 identification of 15 different cell clusters (Figure 1D). The cell clusters were annotated manually
214 using marker genes that were conserved between both conditions as astrocytes, microglia,
215 neurons, endothelial cells, ependymal cells, and mixed glia. We observed an enrichment of glial
216 cells with 96% of all cells detected annotated as either astrocytes, microglia or mixed glia.

217 When assessing the cell distribution between the CNO treated and the negative control
218 groups over the different cell types, we noticed large differences in the percentage of cells in the
219 mixed glia I (30.66% in the saccharin group vs. 45.32% in the CNO group), mixed glia II
220 (29.62% in the saccharin group vs. 14.87% in the CNO group) and microglia II clusters (11.39%
221 in the saccharin group vs. 6.60% in the CNO group, Figure 1E). Smaller differences were
222 observed in the astrocyte (7.41% in the saccharin group vs. 5.30% in the CNO activated group)
223 and microglia I (12.37% in the saccharin group vs. 16.74% in CNO group) clusters (Figure 1E &
224 Supplementary Table 1).

225 ***Re-clustering of the astrocyte cluster showed the presence of transcriptionally different 226 astrocyte types after chronic activation of astrocytes***

227 Since Gq-DREADD was only expressed in astrocytes, we analyzed the effect of Gq-DREADD
228 activation by comparing the genes that were differentially expressed between the saccharin
229 group and the CNO group in the astrocyte cluster. We identified 396 genes that were either up-
230 or downregulated in the CNO group compared to the saccharin group (Figure 2A). Gene
231 enrichment and functional annotation analysis showed that transcripts that were upregulated in
232 the CNO group are involved in myelin sheath biology while the downregulated genes were
233 involved in gene expression and translation (Supplementary Data 1). Network analysis was
234 performed using MetaCore™. We found that 16 of the genes that were upregulated after
235 activation of Gq-DREADD with CNO were in a 50-gene network represented by CMKLR1,
236 SPARCL1, Rich1, Transcobalamin II, OLFML3 (Supplementary Figure 2). The top processes
237 linked to this network were GPCR signaling pathway, ionotropic glutamate receptor signaling
238 pathway, adenylate cyclase inhibiting GPCR signaling pathway, cellular calcium ion
239 homeostasis, and calcium ion homeostasis. Because these cellular processes are downstream
240 pathways regulated by Gq-DREADD, this analysis confirmed the Gq-DREADD-mediated
241 activation of astrocytes.

242 To investigate how activation of astrocytes alters their gene expression in more detail,
243 we re-clustered the astrocyte cluster (Figure 2B). Sub-clustering of the astrocytes showed cell

244 types that were observed in the saccharin group (clusters 0, 2 and 3) while nearly absent from
245 the CNO group, and vice versa (clusters 1 and 4, Figure 2B). This was confirmed by the cell
246 distribution over the different clusters. Cluster 0 accounted for 53.26% of all cells in the
247 saccharin group while only 3.96% in the CNO group. Cluster 1 on the other hand represented
248 only 0.87% in the saccharin group, while 66.55% in the CNO group (Figure 3C, Supplementary
249 Table 2). Gene enrichment and functional annotation analysis of the differentially expressed
250 genes in the astrocytic sub-clusters show different enriched categories for each cluster
251 (Supplementary Data 2). The clusters in the saccharin group (cluster 0, 2 and 3) are enriched
252 for genes involved in regulation of neuronal death, neuroinflammatory response and regulation
253 of synaptic organization, while those of the CNO clusters (cluster 1 and 4) are enriched for
254 genes involved in low-density lipoprotein particles, central nervous system development,
255 gliogenesis, and glial cell differentiation (Supplementary Data 2).

256 ***Re-clustering of the mixed glia cell clusters showed the presence of both microglia-like 257 and astrocyte-like cells in both mixed glia cell clusters***

258 We annotated two cell clusters as 'Mixed Glia' since their conserved marker genes showed an
259 equal likelihood of these cells being annotated as astrocytes or microglia. Activation of
260 astrocytes using CNO led to a 27% increase in cell numbers in the mixed glia I cluster and a
261 56% decrease in the mixed glia II cluster (Figure 1E & Supplementary Table 1).

262 Differentially expressed genes in the mixed glia I cluster showed that activation of
263 astrocytes by the administration of CNO downregulated genes involved in the immune system,
264 system development, cell migration and response to stress (Figure 3A, Supplementary Data 1).
265 Genes that were upregulated after CNO treatment are involved in ribosomal processes, as well
266 as neurodegenerative diseases such as Parkinson's disease, Huntington's disease and
267 Alzheimer's disease (Figure 3A, Supplementary Data 1). In the mixed glia II cluster, gene
268 enrichment and functional annotation of differentially expressed genes demonstrated that
269 downregulated genes were involved in the astrocytic transcription factor AP-1 complex while the
270 genes that were upregulated after hM3Dq activation were mainly involved in ribosomal
271 processes (Figure 3D, Supplementary Data 1).

272 To investigate what cell type is responsible for these effects, we re-clustered both mixed
273 glia clusters. Re-clustering of the mixed glia I cluster resulted in eight different sub-clusters while
274 the re-clustering of the mixed glia II cluster resulted in six sub-clusters (Figure 3B and 3E). Cells
275 belonging to cluster 2 in the mixed glia I group were more abundant in the CNO group
276 compared to the saccharin group. 0.78% of the cells in the saccharin group were part of cluster
277 2, while 10.06% of cells in the CNO group (Figure 3C, Supplementary Table 3). Gene ontology
278 analysis of differentially expressed genes shows that the cells in cluster 2 are involved in
279 lipoprotein particle clearance, lipid transport across the blood-brain barrier and regulation of
280 presynaptic membrane transport (Supplementary Data 3).

281 Re-clustering of the mixed glia II cluster showed more dramatic effects of CNO on the
282 different sub-clusters than was observed in the mixed glia I cluster. Cluster 0 (56.90% in the
283 saccharin group vs. 11.66% in the CNO group), cluster 1 (37.12% in the saccharin group vs.
284 0.87% in the CNO group) and cluster 4 (3.13% in the saccharin group vs. 0.62% in the CNO
285 group) disappeared almost entirely after CNO treatment while cluster 2 (2.69% in the saccharin
286 group vs. 66.26% in the CNO group) and cluster 3 (0.05% in the saccharin group vs. 20.45% in
287 the CNO group) appeared after CNO treatment (Figure 3E & 3F, Supplementary Table 4).
288 Differentially expressed genes in clusters 0, 1 and 4 were involved in the response to axon

289 injury and extracellular stimuli, corticospinal tract atrophy, cell motility, and regulation of the
290 actin cytoskeleton (Supplementary Data 4). The genes that were differentially expressed in
291 clusters 2 and 3 played a role in vitamin B6 levels, aging and the mitochondrial respiratory
292 complex (Supplementary Data 4).

293 ***Chronic activation of astrocytes changed the transcriptome of microglia***

294 Even though Gq-DREADD was only expressed in astrocytes, we observed a 42% decrease in
295 the number of cells in the microglia II cluster after activation of astrocytes with CNO (Figure 1E
296 & Supplementary Table 1). Gene enrichment and functional analysis of genes that were
297 upregulated after CNO treatment in the microglia II cluster were mainly involved in ribosomal
298 processes while the downregulated genes were involved in MAPK activation (Supplementary
299 Data 1).

300 Re-clustering of the microglia II cluster resulted in the identification of seven sub-
301 clusters. Three sub-clusters were mainly observed in the saccharin group (clusters 0, 2 and 3),
302 two were more common in the CNO group (clusters 1 and 4), and two others (clusters 5 and 6)
303 were present in both groups (Figure 4B & 4C, Supplementary Table 5). Differentially expressed
304 genes in clusters 0, 2 and 3 were involved in translation, ribosomal processes, the innate
305 immune system and cell death (Supplementary Data 5). Clusters 1 and 4, on the other hand,
306 were enriched for transcripts involved in the innate immune system, lysosomal functions,
307 synaptic pruning, respiratory chain complex, and response to lipoprotein particles
308 (Supplementary Data 5).

309 The majority of the differentially expressed genes in the other microglial clusters
310 (microglia I, III, IV and V) were upregulated in the CNO group compared to the saccharin group
311 (Figure 5A, 5D, 5G & 5J). The microglia I cluster was highly enriched for differentially expressed
312 genes involved in the negative regulation of cell growth, cellular metabolic processes, and gene
313 expression (Supplementary Data 1). The microglia III cluster was enriched for transcripts
314 involved in the immune system, cytoplasmic organelles such as lysosomes, and cell death
315 (Supplementary Data 1). Both microglia IV and V were highly enriched for genes involved in
316 ribosomal processes (Supplementary Data 1).

317 Re-clustering of the microglia I cluster resulted in seven sub-clusters of which clusters 4
318 and 6 were only observed in the CNO group (Figure 5B & 5C, Supplementary Table 6).
319 Differentially expressed genes in these two clusters were involved in the innate immune system,
320 antigen processing and presentation, and neuronal cell death (Supplementary Data 6).

321 Re-clustering of the microglia III cluster resulted in five sub-clusters (Figure 5E).
322 Although all of them were observed in both groups, cluster 0 was six times more prominent in
323 the saccharin group (56.08%) compared to the CNO group (8.95%), and cluster 2 was nine
324 times more pronounced in the CNO group (36.24%) than in the saccharin group (3.97%, Figure
325 5E & 5F, Supplementary Table 7). The differentially expressed genes in both clusters were
326 involved in the migration of immune cells like neutrophils, granulocytes, and macrophages
327 (Supplementary Data 7).

328 The microglia IV cluster showed five sub-clusters after re-clustering. Clusters 2 and 3
329 were only observed in the saccharin group, and thus, were completely absent from the CNO
330 group (Figure 5H & 5I, Supplementary Table 8). Differentially expressed genes in clusters 2 and
331 3 were shown to be involved in negative regulation of chronic inflammatory response, ribosomal
332 processes, and spine synapse organization (Supplementary Data 8). Clusters 0 (14.67% in the

333 saccharin group vs. 45.09% in the CNO group) and 1 (0.80% in the saccharin group vs. 48.61%
334 in the CNO group) were more common in the CNO group compared to the saccharin group
335 (Figure 5H & 5I, Supplementary Table 8). Differentially expressed genes in these two clusters
336 were involved in cell death, the immune system, and ubiquitination (Supplementary Data 8).

337 Finally, re-clustering of the fifth microglial cluster resulted in four different cell clusters
338 (Figure 5K). Clusters 0 and 2, showed a 1.7 fold increase and a 50% decrease in cell numbers
339 between the saccharin and the CNO groups, respectively (Figure 5L, Supplementary Table 9).
340 The gene enrichment and functional annotation of the differentially expressed genes for clusters
341 0 and 2 showed involvement in ribosomal processes, as well as in neurodegenerative diseases
342 such as Parkinson's disease and Alzheimer's disease (Supplementary Data 9).

343 ***Long-term activation of astrocytes have no major effects on the transcriptome of*** 344 ***neurons***

345 To study whether Gq-DREADD-induced activation of astrocytes results in transcriptional
346 changes in neurons, we re-clustered the neuronal cluster. Three clusters were identified that
347 were observed in both groups (Figure 6A). Cluster 0 showed a small decrease and cluster 2 a
348 small increase in number of cells after astrocyte activation with Gq-DREADD, while no
349 difference was observed in cluster 1 (Figure 6A & 6B, Supplementary Table 10). Genes that
350 were differentially expressed in clusters 0 and 2 are both involved in nervous system
351 development, and specifically in neurogenesis, suggesting that both cell types are not
352 biologically different. The genes that were differentially expressed in cluster 1 are mainly
353 involved in ribosomal processes (Supplemental Data 10).

354 **Discussion**

355 To the best of our knowledge, this is the first study to show transcriptional changes in glia that
356 occur after long-term activation of astrocytes with the Gq-DREADD in an *in vivo* model.
357 Previous studies have expressed the Gq-DREADD specifically in astrocytes using the GFAP
358 promotor and showed an increase in intracellular Ca²⁺ after activation with CNO (Agulhon, Boyt
359 et al. 2013, Bull, Freitas et al. 2014, Scofield, Boger et al. 2015). However, none of these
360 studies looked at the effect of Gq-DREADD activation on the transcriptome of astrocytes or
361 other brain cells such as neurons or microglia. To determine the effect of long-term activation of
362 astrocytes through Gq-DREADD, we performed scRNA seq on hippocampal and cortical cells of
363 wild type mice that selectively expressed Gq-DREADD in astrocytes. Network analysis of the
364 genes that were upregulated after Gq-DREADD activation with CNO in astrocytes showed an
365 involvement of these genes in the GPCR signaling pathway and calcium homeostasis. These
366 findings confirmed the transcriptionally activated state of the astrocytes after long-term
367 activation of Gq-DREADD with CNO (Supplementary Figure 2). Furthermore, our results
368 demonstrate the presence of transcriptionally different astrocyte populations after Gq-DREADD
369 activation with CNO compared to the control group. Although the up- or downregulation of
370 differentially expressed genes was relatively low, we could clearly observe transcriptionally
371 different astrocytic sub-clusters. While some clusters were predominantly present in the control
372 group, other were mainly observed after activation with CNO (Figure 2B). We also observed that
373 our astrocyte population in the CNO group did not show the transcriptional profile of reactive
374 astrogliosis that is typically seen in neurodegenerative diseases (Supplementary Figure 3)
375 (Kraft, Hu et al. 2013). Therefore, we hypothesize that long-term activation of astrocytes
376 changes their transcriptional profile to a new steady state phenotype. Further research is

377 needed to assess what this new steady state phenotype means to the astrocytes and their
378 environment, and their biological relevance.

379 Gene and functional analysis of the astrocyte subclusters showed a functional difference
380 between the astrocytes present in the control group and after Gq-DREADD activation
381 (Supplementary Data 2). The astrocyte clusters that were more abundant in the control group
382 than in the CNO group (clusters 0, 2 & 3, Figure 2B) were involved in the regulation of several
383 processes such as transport, neuronal cell death, and synapse structure and activity
384 (Supplementary Data 2). The cell clusters that were more abundant in the CNO group (clusters
385 1 & 4, Figure 2B) were important for low-density lipoprotein homeostasis and central nervous
386 system development. Strikingly, gene ontology showed that the differentially expressed genes
387 from the CNO subclusters were enriched for glial cell development, astrocyte differentiation and
388 negative regulation of neuronal apoptotic processes (Supplementary Data 2). While the
389 astrocytes enriched in the control group show a homeostatic phenotype, the phenotype for the
390 astrocytes enriched in the CNO group is less clear (Barres 2008). Previous research has shown
391 that the transcriptomic profile of astrocytes varied in response to different “insults”, e.g. long-
392 term activation (Hamby, Coppola *et al.* 2012, Anderson, Ao *et al.* 2014). Therefore, additional
393 research is needed to elucidate the exact molecular phenotype of the Gq-DREADD activated-
394 astrocytes.

395 Interestingly, the transcriptome of microglia was dramatically affected by the long-term
396 activation of astrocytes (Figures 4 and 5). We observed microglial clusters that were absent in
397 the control group and dominating in the CNO group (Figures 5B & 5H). Furthermore, the
398 transcriptomic changes that occurred in microglial cells after Gq-DREADD activation were
399 different than those in control microglia (Supplementary Data 5-9). After long-term activation of
400 astrocytes, microglia became involved in synaptic pruning, lipoprotein particle processes, and
401 migration and chemotaxis of immune cells. In addition, our data demonstrated that long-term
402 activation of astrocytes had no significant effect on the transcriptome of neurons. However
403 caution is warranted when interpreting this data since less than 1% of our total cell population
404 subsists of neurons (Supplementary Table 1).

405 Our single cell dissociation protocol shows a significant enrichment of glial cells and a
406 relative depletion of neurons. Possible explanations for this glial enrichment are (1) the fact that
407 we dissociated brain tissue of four months-old mice. Previous studies mostly perform scRNA
408 seq in younger mice while single nucleus RNA sequencing is more common in adult mice
409 (Zeisel, Munoz-Manchado *et al.* 2015, Hook, McClymont *et al.* 2018, Loo, Simon *et al.* 2019,
410 Zhou, Song *et al.* 2020). The central nervous system of older mice is more complex than that of
411 younger mice, making it harder to dissociate it into single cells, and as a result some cell types
412 can get over- or underrepresented (Grindberg, Yee-Greenbaum *et al.* 2013, Darmanis, Sloan *et al.*
413 2015, Krishnaswami, Grindberg *et al.* 2016, Lake, Ai *et al.* 2016, Lake, Codeluppi *et al.* 2017,
414 Tasic, Yao *et al.* 2018). (2) To arrest ongoing gene expression and to decrease the likelihood of
415 inducing heat shock proteins or immediate-early response genes, we performed our dissociation
416 protocol at 4°C instead of 37°C. However, one drawback of an ice-cold dissociation is the
417 decrease in efficiency of dissociation with certain tissues, such as the brain (Adam, Potter *et al.*
418 2017, van den Brink, Sage *et al.* 2017, Denisenko, Guo *et al.* 2019). As such, one might
419 hypothesize that ice-cold dissociation was not capable of breaking neuronal connections, while
420 the connections formed by glial cells were easier to break.

421 In summary, our data show for the first time the effect of long-term activation of
422 astrocytes with Gq- DREADD. We have shown that prolonged activation of astrocytes change
423 the transcriptional profile of astrocytes and microglia in the brain, while there is little to no effect
424 on neurons. Our findings are also important for the interpretation of future studies using Gq-
425 DREADD activation in astrocytes. Furthermore, our data provides an important resource for
426 future chemogenetic studies.

427 **Data availability**

428 Full list of differentially expressed genes and the g:Profiler analysis are provided online as
429 Supplementary Data. The Raw sequencing data will be made publicly available through the
430 GEO database.

431 **Acknowledgments**

432 We thank Dr. John Fryer and Jonathon Sens for single-cell isolation protocol and Dr. Leonard
433 Petrucelli, Karen Jansen-West, and Lillian Daugherty for virus packaging of the plasmid
434 (Department of Neuroscience, Mayo Clinic). This publication was made possible by the Stark
435 Neurosciences Research Institute, the Indiana Alzheimer Disease Center, Eli Lilly and
436 Company, and by the Indiana Clinical and Translational Sciences Institute, funded in part by
437 grant # UL1TR002529 from the NIH, National Center for Advancing Translational Sciences.
438 Sequencing on an Illumina NovaSeq SP was carried out in the Center for Medical Genomics at
439 Indiana University School of Medicine, which is partially supported by the Indiana Genomic
440 Initiative at Indiana University (INGEN); INGEN is supported in part by the Lilly Endowment, Inc.
441 The authors also acknowledge the Indiana University Pervasive Technology Institute for
442 providing Carbonate supercomputer resources that have contributed to the research results
443 reported within this paper (URL: <https://pti.iu.edu/>, Stewart, C.A., Welch, V., Plale, B., Fox, G.,
444 Pierce, M., Sterling, T. (2017). Indiana University Pervasive Technology Institute. Bloomington,
445 IN. <https://doi.org/10.5967/K8G44NGB>). This work was also supported in part by grants from
446 Strategic Research Initiative, Precision Health Initiative (Indiana University), NIH
447 R01AG054102, R01AG053500, R01AG053242, and R21AG050804. This material is based
448 upon work supported by the National Science Foundation under Grant No. CNS-0521433. This
449 work was supported in part by Shared University Research grants from IBM, Inc., to Indiana
450 University. The content is solely the responsibility of the authors and does not necessarily
451 represent the official views of the National Institutes of Health, National Science Foundation or
452 Eli Lilly and Company. Figure 1A uses an image from Servier Medical Art, Servier Co.

453 **Figure legends**

454 **Figure 1: scRNA sequencing shows differences in cell distribution in the hippocampus**
455 **and cortex of Gq-DREADD-injected mice. (A)** Schematic presentation of the scRNA seq
456 workflow. Male C57BL/6J mice were transduced with AAV5-GFAP-hM3D(Gq) at 8 weeks of
457 age and treated with saccharin or CNO in drinking water for 8 weeks. **(B)** Representative
458 fluorescence images of the hippocampus and cortex demonstrating Gq-DREADD virus spread
459 (red; mCherry) and astrocytes (green; GFAP). Cell nuclei are indicated by blue fluorescence
460 (DAPI). **(C)** Magnified view (from white box in **(B)**) demonstrating mCherry specificity to
461 astrocytes. **(D)** UMAP plot showing the detected cell types in the anterior hippocampus and
462 anterior cortex of C57BL/6J mice. Cluster names were assigned using conserved marker genes.
463 **(E)** The cell distribution of the detected cell clusters in the saccharin and CNO group.

464 **Figure 2: Re-clustering of the astrocyte cell cluster shows the presence of**
465 **transcriptionally different astrocytes after astrocyte-specific activation with the Gq-**
466 **DREADD. (A)** Volcano plot showing differentially expressed genes between the saccharin
467 group and the CNO group in the astrocyte cluster. Differentially expressed genes with an
468 adjusted p value < 0.05 after Bonferonni correction are shown in red. **(B)** UMAP showing the six
469 clusters identified after re-clustering the astrocyte cluster (2,238 cells). The UMAP is split into
470 two groups, the saccharin group (1,380 cells) and the CNO group (858 cells). **(C)** Bar graph
471 showing the cell distribution over the different astrocytic sub-clusters.

472 **Figure 3: Re-clustering of the mixed glia cell clusters shows transcriptionally different**
473 **cell types after activation of astrocytes with the Gq-DREADD. (A & D)** Volcano plot showing
474 differentially expressed genes between the saccharin control group and the CNO group in the
475 mixed glia I **(A)** and II **(D)** clusters. Differentially expressed genes with an adjusted p value <
476 0.05 after Bonferonni correction are shown in red. **(B)** UMAP showing the eight clusters
477 identified after re-clustering the mixed glia I cluster (13,029 cells). The UMAP is split into two
478 groups, the saccharin group (5,744 cells) and the CNO group (7,285 cells)). **(C & F)** Bar graph
479 showing the cell distribution over the different mixed glial I **(C)** and II **(F)** sub-clusters. **(E)** UMAP
480 showing the six clusters identified after re-clustering the mixed glia II cluster (7,905 cells). The
481 UMAP is split into two groups, the saccharin group (5,504 cells) and the CNO group (2,401
482 cells).

483 **Figure 4: Re-clustering of the microglia II cell cluster shows the presence of**
484 **transcriptionally different microglia after astrocyte-specific activation with the Gq-**
485 **DREADD. (A)** Volcano plot showing differentially expressed genes between the saccharin
486 group and the CNO group in the microglia II cluster. Differentially expressed genes with an
487 adjusted p value < 0.05 after Bonferonni correction are shown in red. **(B)** UMAP showing the
488 seven clusters identified after re-clustering the microglia II cluster (3,172 cells). The UMAP is
489 split into two groups, the saccharin group (2,107 cells) and the CNO group (1,065 cells). **(C)** Bar
490 graph showing the cell distribution over the different microglia II sub-clusters.

491 **Figure 5: Re-clustering of the microglia I, III, IV and V cell clusters shows**
492 **transcriptionally different cell types after activation of astrocytes with the Gq-DREADD.**
493 **(A, D, G & J)** Volcano plots showing differentially expressed genes between the saccharin
494 group and the CNO group in the microglia I **(A)**, microglia III **(D)**, microglia IV **(G)**, microglia V
495 **(J)** clusters. Differentially expressed genes with an adjusted p value < 0.05 after Bonferonni
496 correction are shown in red. **(B, E, H & K)** UMAP showing the different clusters that were
497 identified after re-clustering the microglia I (4,987 cells, **(B)**), III (861 cells, **(E)**), IV (823 cells,
498 **(H)**) and V (243 cells, **(K)**) clusters. The UMAP is split into two groups, the saccharin group and
499 the CNO group (cluster I (2,293 vs. 2,694 cells **(C)**), III (403 vs. 458 cells **(F)**), IV (375 vs. 448
500 cells **(I)**) & V (118 vs. 125 cells **(L)**). Bar graph showing the cell distribution over the different
501 microglial sub-clusters (I **(C)**, III **(F)**, IV **(I)** and V **(L)**).

502 **Figure 6: Re-clustering of the neuron cell cluster shows no effect after astrocyte-specific**
503 **activation with the Gq-DREADD. (A)** UMAP showing the three clusters identified after re-
504 clustering the neuron cluster (239 cells). The UMAP is split into two groups, the saccharin group
505 (108 cells) and the CNO group (131 cells). **(B)** Bar graph showing the cell distribution over the
506 different neuronal sub-clusters.

507

508 **References**

- 509 Abbott, N. J., L. Rönnbäck and E. Hansson (2006). "Astrocyte–endothelial interactions at the
510 blood–brain barrier." Nature Reviews Neuroscience **7**(1): 41-53.
- 511 Adam, M., A. S. Potter and S. S. Potter (2017). "Psychrophilic proteases dramatically reduce
512 single-cell RNA-seq artifacts: a molecular atlas of kidney development." Development **144**(19):
513 3625-3632.
- 514 Agulhon, C., K. M. Boyt, A. X. Xie, F. Friocourt, B. L. Roth and K. D. McCarthy (2013).
515 "Modulation of the autonomic nervous system and behaviour by acute glial cell Gq protein-
516 coupled receptor activation in vivo." J Physiol **591**(22): 5599-5609.
- 517 Anderson, M. A., Y. Ao and M. V. Sofroniew (2014). "Heterogeneity of reactive astrocytes."
518 Neuroscience Letters **565**: 23-29.
- 519 Armbruster, B. N., X. Li, M. H. Pausch, S. Herlitze and B. L. Roth (2007). "Evolving the lock to fit
520 the key to create a family of G protein-coupled receptors potently activated by an inert ligand."
521 Proceedings of the National Academy of Sciences **104**(12): 5163-5168.
- 522 Arneson, D., G. Zhang, Z. Ying, Y. Zhuang, H. R. Byun, I. S. Ahn, F. Gomez-Pinilla and X. Yang
523 (2018). "Single cell molecular alterations reveal target cells and pathways of concussive brain
524 injury." Nat Commun **9**(1): 3894.
- 525 Barres, B. A. (2008). "The mystery and magic of glia: a perspective on their roles in health and
526 disease." Neuron **60**(3): 430-440.
- 527 Batiuk, M. Y., A. Martirosyan, J. Wahis, F. de Vin, C. Marneffe, C. Kusserow, J. Koeppen, J. F.
528 Viana, J. F. Oliveira, T. Voet, C. P. Ponting, T. G. Belgard and M. G. Holt (2020). "Identification
529 of region-specific astrocyte subtypes at single cell resolution." Nature Communications **11**(1):
530 1220.
- 531 Benediktsson, A. M., S. J. Schachtele, S. H. Green and M. E. Dailey (2005). "Ballistic labeling
532 and dynamic imaging of astrocytes in organotypic hippocampal slice cultures." J Neurosci
533 Methods **141**(1): 41-53.
- 534 Bull, C., K. C. Freitas, S. Zou, R. S. Poland, W. A. Syed, D. J. Urban, S. C. Minter, K. L.
535 Shelton, K. F. Hauser and S. S. Negus (2014). "Rat nucleus accumbens core astrocytes
536 modulate reward and the motivation to self-administer ethanol after abstinence."
537 Neuropsychopharmacology **39**(12): 2835-2845.
- 538 Bull, C., K. C. Freitas, S. Zou, R. S. Poland, W. A. Syed, D. J. Urban, S. C. Minter, K. L.
539 Shelton, K. F. Hauser, S. S. Negus, P. E. Knapp and M. S. Bowers (2014). "Rat nucleus
540 accumbens core astrocytes modulate reward and the motivation to self-administer ethanol after
541 abstinence." Neuropsychopharmacology **39**(12): 2835-2845.
- 542 Bushong, E. A., M. E. Martone, Y. Z. Jones and M. H. Ellisman (2002). "Protoplasmic astrocytes
543 in CA1 stratum radiatum occupy separate anatomical domains." J Neurosci **22**(1): 183-192.
- 544 Butler, A., P. Hoffman, P. Smibert, E. Papalexi and R. Satija (2018). "Integrating single-cell
545 transcriptomic data across different conditions, technologies, and species." Nat Biotechnol
546 **36**(5): 411-420.

- 547 Darmanis, S., S. A. Sloan, Y. Zhang, M. Enge, C. Caneda, L. M. Shuer, M. G. Hayden Gephart,
548 B. A. Barres and S. R. Quake (2015). "A survey of human brain transcriptome diversity at the
549 single cell level." Proceedings of the National Academy of Sciences **112**(23): 7285-7290.
- 550 Denisenko, E., B. B. Guo, M. Jones, R. Hou, L. de Kock, T. Lassmann, D. Poppe, O. Clement,
551 R. K. Simmons, R. Lister and A. R. R. Forrest (2019). "Systematic bias assessment in solid
552 tissue 10x scRNA-seq workflows." bioRxiv: 832444.
- 553 Drinkut, A., Y. Tereshchenko, J. B. Schulz, M. Bähr and S. Kügler (2012). "Efficient gene
554 therapy for Parkinson's disease using astrocytes as hosts for localized neurotrophic factor
555 delivery." Molecular therapy **20**(3): 534-543.
- 556 Grindberg, R. V., J. L. Yee-Greenbaum, M. J. McConnell, M. Novotny, A. L. O'Shaughnessy, G.
557 M. Lambert, M. J. Arauzo-Bravo, J. Lee, M. Fishman, G. E. Robbins, X. Lin, P. Venepally, J. H.
558 Badger, D. W. Galbraith, F. H. Gage and R. S. Lasken (2013). "RNA-sequencing from single
559 nuclei." Proc Natl Acad Sci U S A **110**(49): 19802-19807.
- 560 Hamby, M. E., G. Coppola, Y. Ao, D. H. Geschwind, B. S. Khakh and M. V. Sofroniew (2012).
561 "Inflammatory Mediators Alter the Astrocyte Transcriptome and Calcium Signaling Elicited by
562 Multiple G-Protein-Coupled Receptors." The Journal of Neuroscience **32**(42): 14489-14510.
- 563 Hook, P. W., S. A. McClymont, G. H. Cannon, W. D. Law, A. J. Morton, L. A. Goff and A. S.
564 McCallion (2018). "Single-Cell RNA-Seq of Mouse Dopaminergic Neurons Informs Candidate
565 Gene Selection for Sporadic Parkinson Disease." Am J Hum Genet **102**(3): 427-446.
- 566 Keren-Shaul, H., A. Spinrad, A. Weiner, O. Matcovitch-Natan, R. Dvir-Szternfeld, T. K. Ulland,
567 E. David, K. Baruch, D. Lara-Astaiso, B. Toth, S. Itzkovitz, M. Colonna, M. Schwartz and I. Amit
568 (2017). "A Unique Microglia Type Associated with Restricting Development of Alzheimer's
569 Disease." Cell **169**(7): 1276-1290 e1217.
- 570 Kraft, A. W., X. Hu, H. Yoon, P. Yan, Q. Xiao, Y. Wang, S. C. Gil, J. Brown, U. Wilhelmsson, J.
571 L. Restivo, J. R. Cirrito, D. M. Holtzman, J. Kim, M. Pekny and J. M. Lee (2013). "Attenuating
572 astrocyte activation accelerates plaque pathogenesis in APP/PS1 mice." FASEB J **27**(1): 187-
573 198.
- 574 Krishnaswami, S. R., R. V. Grindberg, M. Novotny, P. Venepally, B. Lacar, K. Bhutani, S. B.
575 Linker, S. Pham, J. A. Erwin, J. A. Miller, R. Hodge, J. K. McCarthy, M. Kelder, J. McCarrison,
576 B. D. Aevermann, F. D. Fuertes, R. H. Scheuermann, J. Lee, E. S. Lein, N. Schork, M. J.
577 McConnell, F. H. Gage and R. S. Lasken (2016). "Using single nuclei for RNA-seq to capture
578 the transcriptome of postmortem neurons." Nat Protoc **11**(3): 499-524.
- 579 Lake, B. B., R. Ai, G. E. Kaeser, N. S. Salathia, Y. C. Yung, R. Liu, A. Wildberg, D. Gao, H. L.
580 Fung, S. Chen, R. Vijayaraghavan, J. Wong, A. Chen, X. Sheng, F. Kaper, R. Shen, M.
581 Ronaghi, J. B. Fan, W. Wang, J. Chun and K. Zhang (2016). "Neuronal subtypes and diversity
582 revealed by single-nucleus RNA sequencing of the human brain." Science **352**(6293): 1586-
583 1590.
- 584 Lake, B. B., S. Codeluppi, Y. C. Yung, D. Gao, J. Chun, P. V. Kharchenko, S. Linnarsson and K.
585 Zhang (2017). "A comparative strategy for single-nucleus and single-cell transcriptomes
586 confirms accuracy in predicted cell-type expression from nuclear RNA." Scientific Reports **7**(1):
587 6031.

- 588 Lee, H.-M., P. M. Giguere and B. L. Roth (2014). "DREADDs: novel tools for drug discovery and
589 development." Drug discovery today **19**(4): 469-473.
- 590 Liddelow, S. A. and B. A. Barres (2017). "Reactive astrocytes: production, function, and
591 therapeutic potential." Immunity **46**(6): 957-967.
- 592 Loo, L., J. M. Simon, L. Xing, E. S. McCoy, J. K. Niehaus, J. Guo, E. S. Anton and M. J. Zylka
593 (2019). "Single-cell transcriptomic analysis of mouse neocortical development." Nat Commun
594 **10**(1): 134.
- 595 Merienne, N., J. Le Douce, E. Faivre, N. Déglon and G. Bonvento (2013). "Efficient gene
596 delivery and selective transduction of astrocytes in the mammalian brain using viral vectors."
597 Frontiers in cellular neuroscience **7**: 106.
- 598 Raudvere, U., L. Kolberg, I. Kuzmin, T. Arak, P. Adler, H. Peterson and J. Vilo (2019).
599 "g:Profiler: a web server for functional enrichment analysis and conversions of gene lists (2019
600 update)." Nucleic Acids Res **47**(W1): W191-W198.
- 601 Ridet, J., A. Privat, S. Malhotra and F. Gage (1997). "Reactive astrocytes: cellular and
602 molecular cues to biological function." Trends in neurosciences **20**(12): 570-577.
- 603 Rogan, S. C. and B. L. Roth (2011). "Remote control of neuronal signaling." Pharmacological
604 reviews **63**(2): 291-315.
- 605 Roth, B. L. (2016). "DREADDs for neuroscientists." Neuron **89**(4): 683-694.
- 606 Scofield, M. D., H. A. Boger, R. J. Smith, H. Li, P. G. Haydon and P. W. Kalivas (2015). "Gq-
607 DREADD Selectively Initiates Glial Glutamate Release and Inhibits Cue-induced Cocaine
608 Seeking." Biol Psychiatry **78**(7): 441-451.
- 609 Scofield, M. D., H. A. Boger, R. J. Smith, H. Li, P. G. Haydon and P. W. Kalivas (2015). "Gq-
610 DREADD selectively initiates glial glutamate release and inhibits cue-induced cocaine seeking."
611 Biological psychiatry **78**(7): 441-451.
- 612 Sofroniew, M. V. and H. V. Vinters (2010). "Astrocytes: biology and pathology." Acta
613 neuropathologica **119**(1): 7-35.
- 614 Stuart, T., A. Butler, P. Hoffman, C. Hafemeister, E. Papalexi, W. M. Mauck, 3rd, Y. Hao, M.
615 Stoeckius, P. Smibert and R. Satija (2019). "Comprehensive Integration of Single-Cell Data."
616 Cell **177**(7): 1888-1902 e1821.
- 617 Tasic, B., Z. Yao, L. T. Graybiel, K. A. Smith, T. N. Nguyen, D. Bertagnolli, J. Goldy, E. Garren,
618 M. N. Economou, S. Viswanathan, O. Penn, T. Bakken, V. Menon, J. Miller, O. Fong, K. E.
619 Hirokawa, K. Lathia, C. Rimorin, M. Tieu, R. Larsen, T. Casper, E. Barkan, M. Kroll, S. Parry, N.
620 V. Shapovalova, D. Hirschstein, J. Pendergraft, H. A. Sullivan, T. K. Kim, A. Szafer, N. Dee, P.
621 Groblewski, I. Wickersham, A. Cetin, J. A. Harris, B. P. Levi, S. M. Sunkin, L. Madisen, T. L.
622 Daigle, L. Looger, A. Bernard, J. Phillips, E. Lein, M. Hawrylycz, K. Svoboda, A. R. Jones, C.
623 Koch and H. Zeng (2018). "Shared and distinct transcriptomic cell types across neocortical
624 areas." Nature **563**(7729): 72-78.

- 625 Urban, D. J. and B. L. Roth (2015). "DREADDs (designer receptors exclusively activated by
626 designer drugs): chemogenetic tools with therapeutic utility." Annual review of pharmacology
627 and toxicology **55**: 399-417.
- 628 van den Brink, S. C., F. Sage, A. Vertesy, B. Spanjaard, J. Peterson-Maduro, C. S. Baron, C.
629 Robin and A. van Oudenaarden (2017). "Single-cell sequencing reveals dissociation-induced
630 gene expression in tissue subpopulations." Nat Methods **14**(10): 935-936.
- 631 Zamanian, J. L., L. Xu, L. C. Foo, N. Nouri, L. Zhou, R. G. Giffard and B. A. Barres (2012).
632 "Genomic Analysis of Reactive Astroglia." The Journal of Neuroscience **32**(18): 6391-6410.
- 633 Zeisel, A., A. B. Munoz-Manchado, S. Codeluppi, P. Lonnerberg, G. La Manno, A. Jureus, S.
634 Marques, H. Munguba, L. He, C. Betsholtz, C. Rolny, G. Castelo-Branco, J. Hjerling-Leffler and
635 S. Linnarsson (2015). "Brain structure. Cell types in the mouse cortex and hippocampus
636 revealed by single-cell RNA-seq." Science **347**(6226): 1138-1142.
- 637 Zhou, Y., W. M. Song, P. S. Andhey, A. Swain, T. Levy, K. R. Miller, P. L. Poliani, M. Cominelli,
638 S. Grover, S. Gilfillan, M. Cella, T. K. Ulland, K. Zaitsev, A. Miyashita, T. Ikeuchi, M. Sainouchi,
639 A. Kakita, D. A. Bennett, J. A. Schneider, M. R. Nichols, S. A. Beausoleil, J. D. Ulrich, D. M.
640 Holtzman, M. N. Artyomov and M. Colonna (2020). "Human and mouse single-nucleus
641 transcriptomics reveal TREM2-dependent and TREM2-independent cellular responses in
642 Alzheimer's disease." Nature Medicine **26**(1): 131-142.
- 643 Zolotukhin, S., B. Byrne, E. Mason, I. Zolotukhin, M. Potter, K. Chesnut, C. Summerford, R.
644 Samulski and N. Muzyczka (1999). "Recombinant adeno-associated virus purification using
645 novel methods improves infectious titer and yield." Gene therapy **6**(6): 973-985.
- 646

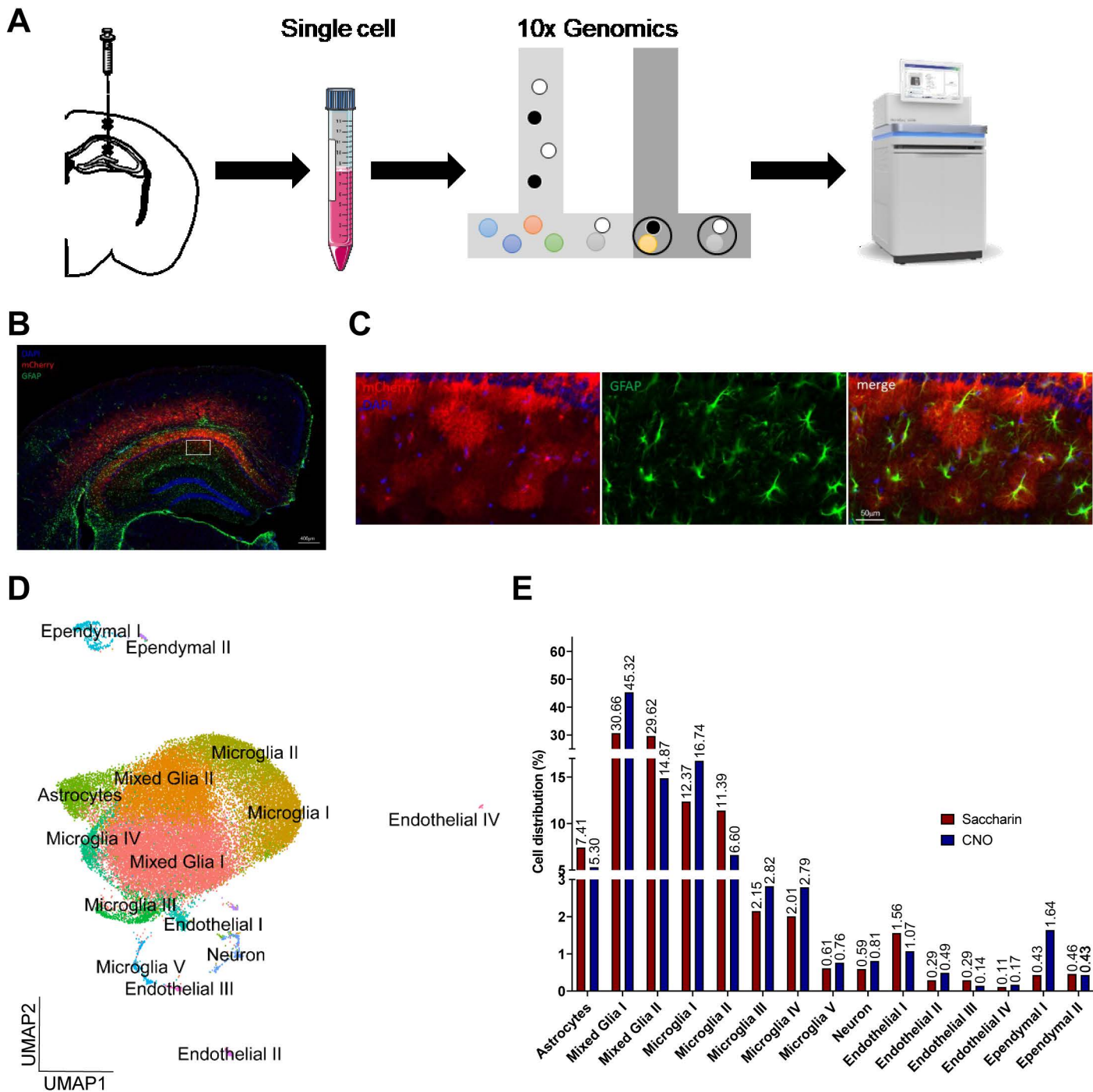


Figure 2

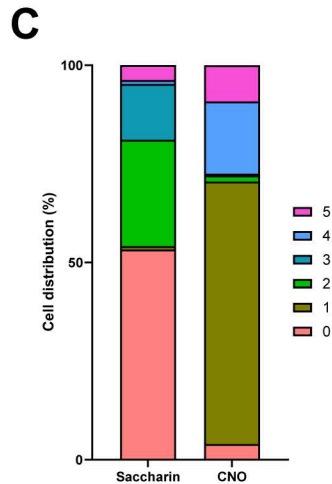
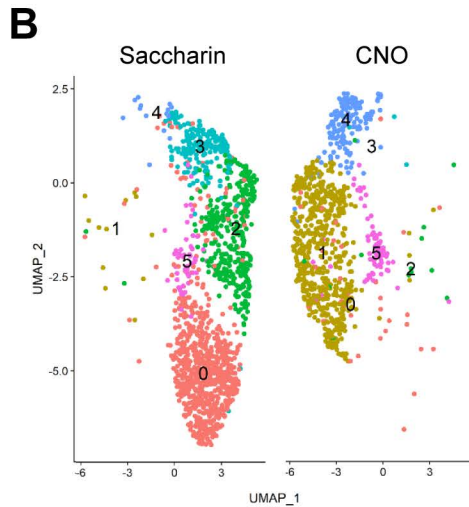
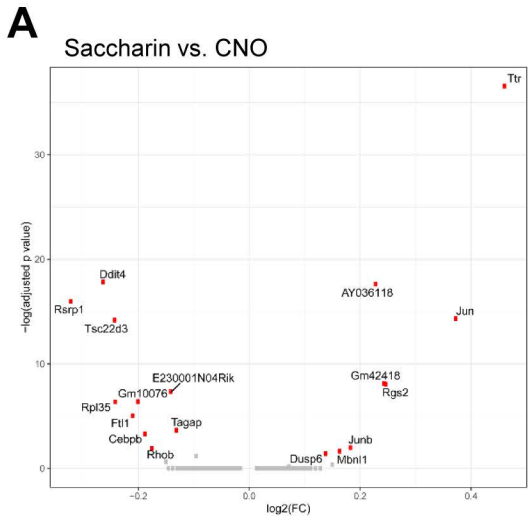


Figure 3

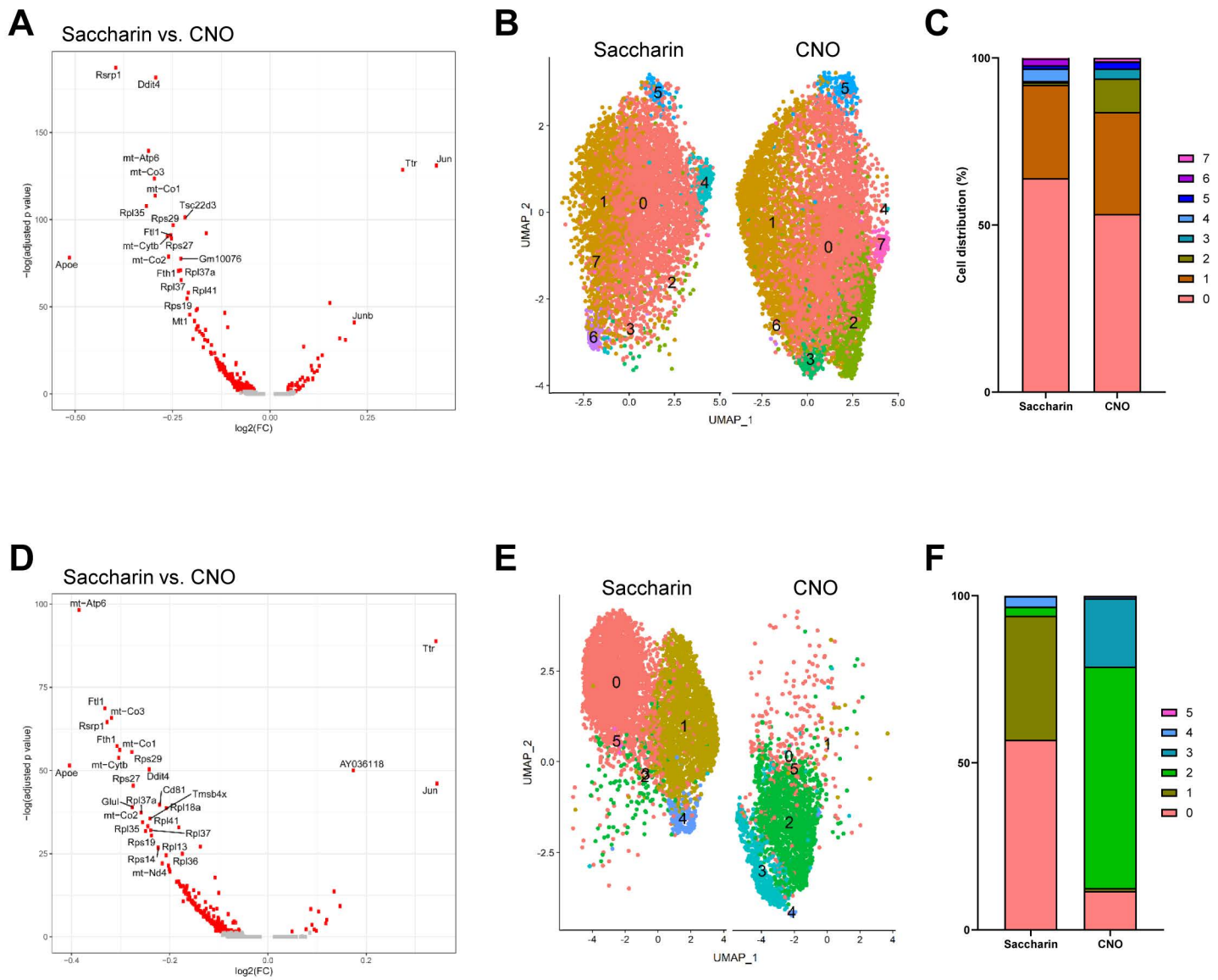
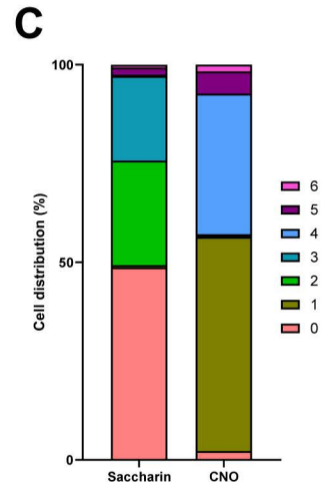
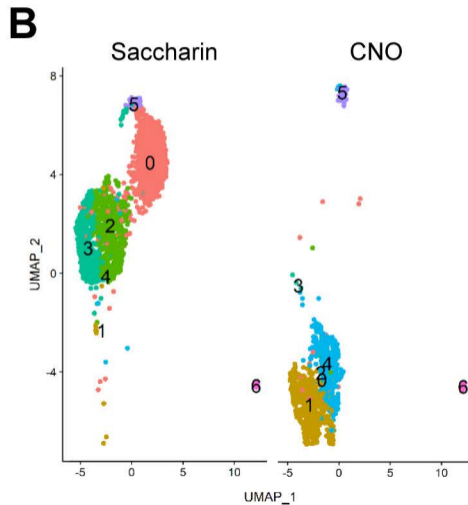
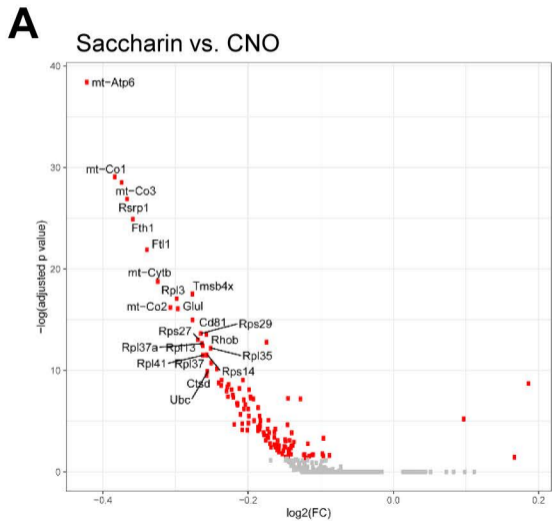


Figure 4



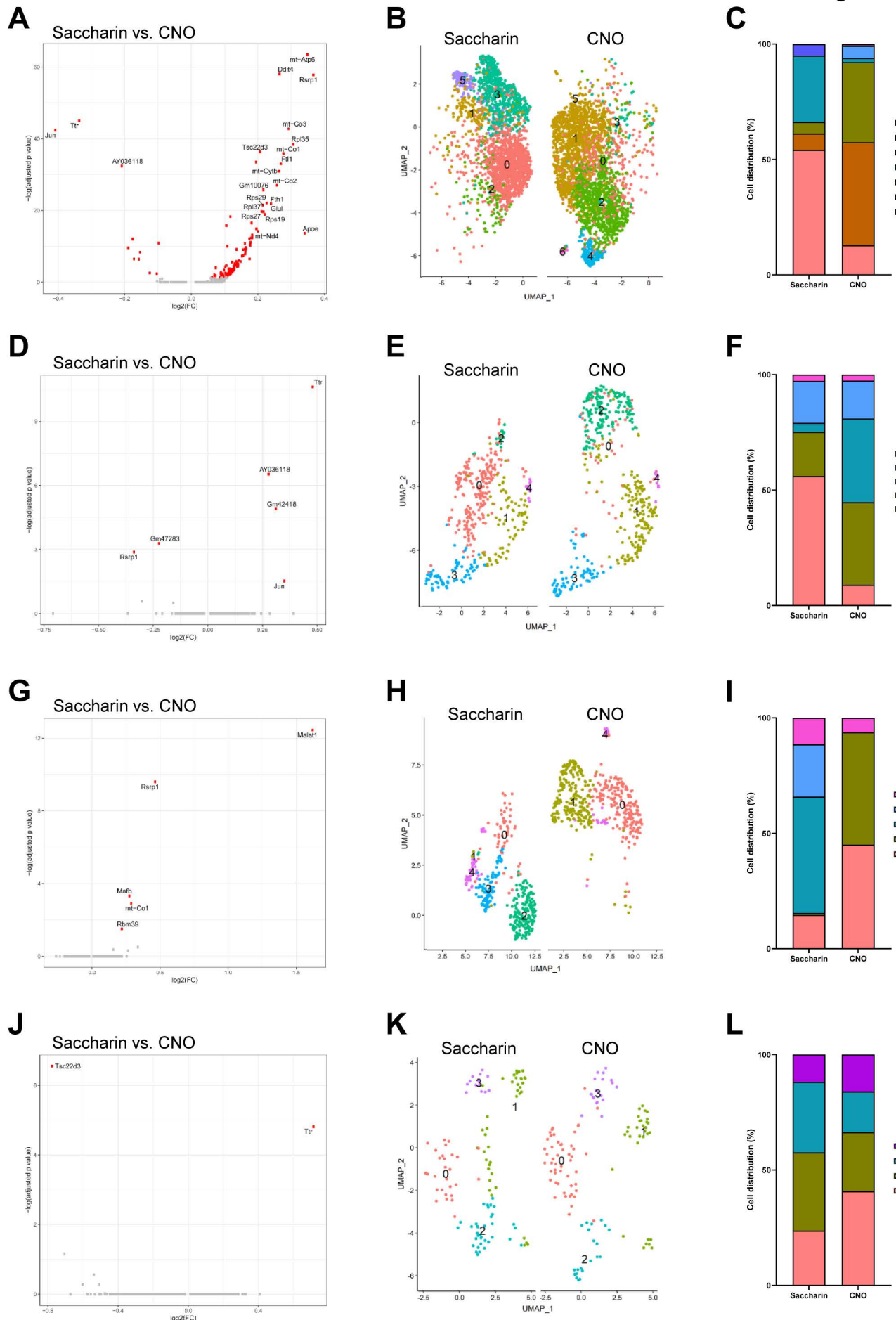
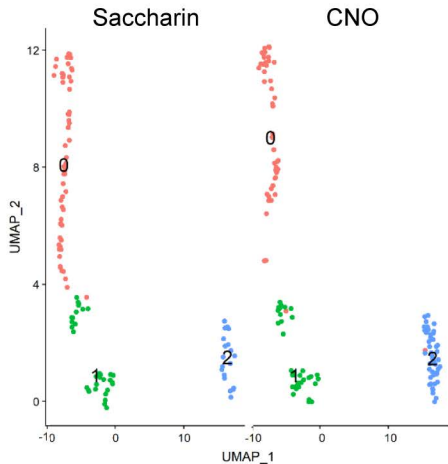
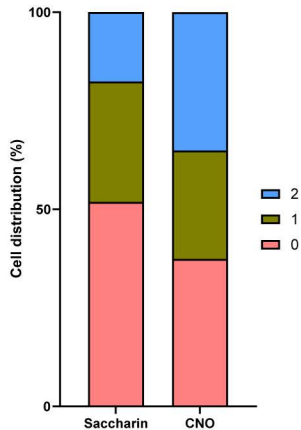


Figure 6

A



B



Chemogenetic activation of astrocytes in the hippocampus and cortex changes the transcriptome of microglia and other cell types.

Stéphanie Philtjens^{1,2#}, Marion T. Turnbull^{3,4#}, Brian P. Thedy³, Younghye Moon^{1,2}, Jungsu Kim^{1,2*}

#Equal contribution

¹Department of Medical and Molecular Genetics, Indiana University School of Medicine, Indianapolis, IN 46202, USA

²Stark Neuroscience Research Institute, Indiana University School of Medicine, Indianapolis, IN 46202, USA

³Department of Neurology, Mayo Clinic, Jacksonville, FL 32224, USA

⁴Department of Neuroscience, Mayo Clinic, Jacksonville, FL 32224, USA

*Corresponding author:

Jungsu Kim, Ph.D.

320 W. 15th Street, NB Bldg Rm 102A

Indianapolis, IN 46202

Phone: 317-278-6351

Fax: 317-274-0067

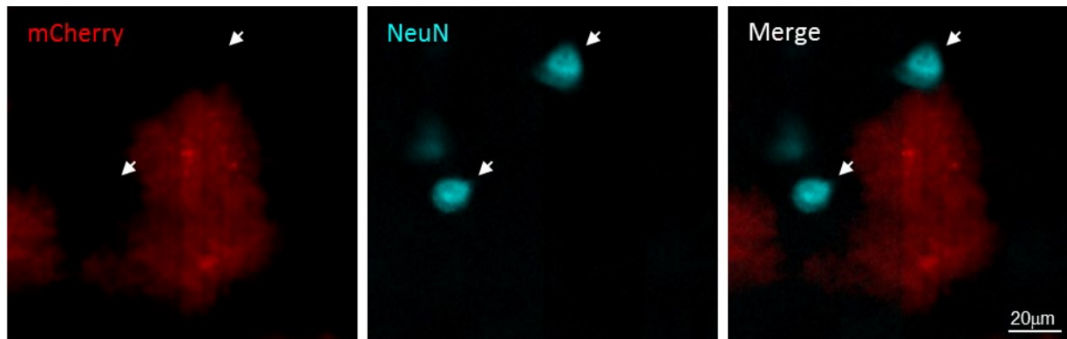
Email: jk123@iu.edu

Key words:

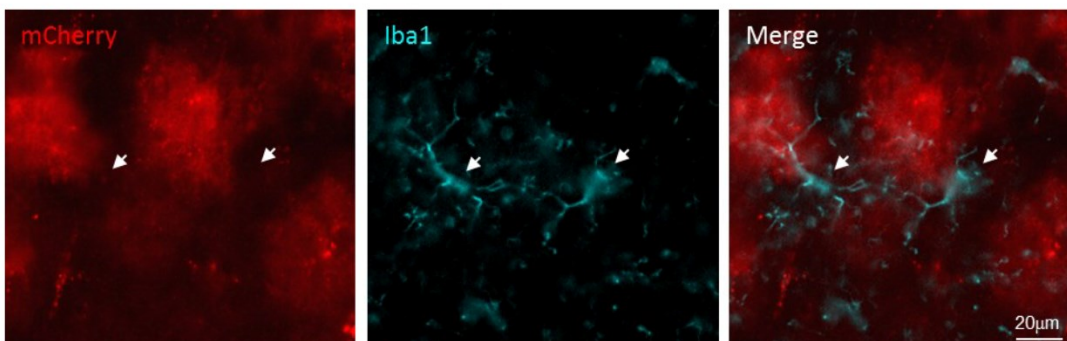
single cell RNA sequencing – DREADDS – astrocytes – microglia – chemogenetics

Supplementary Figure

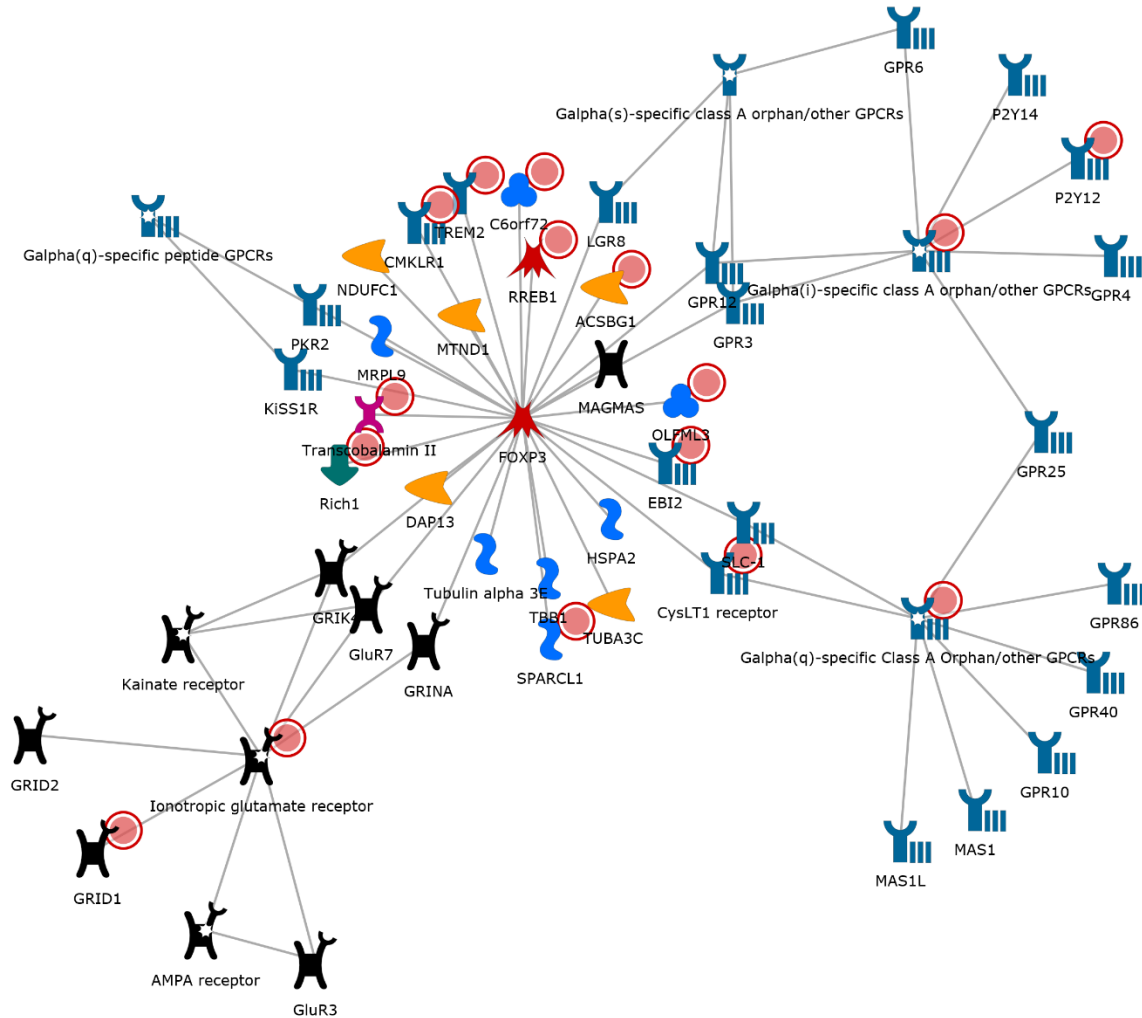
A



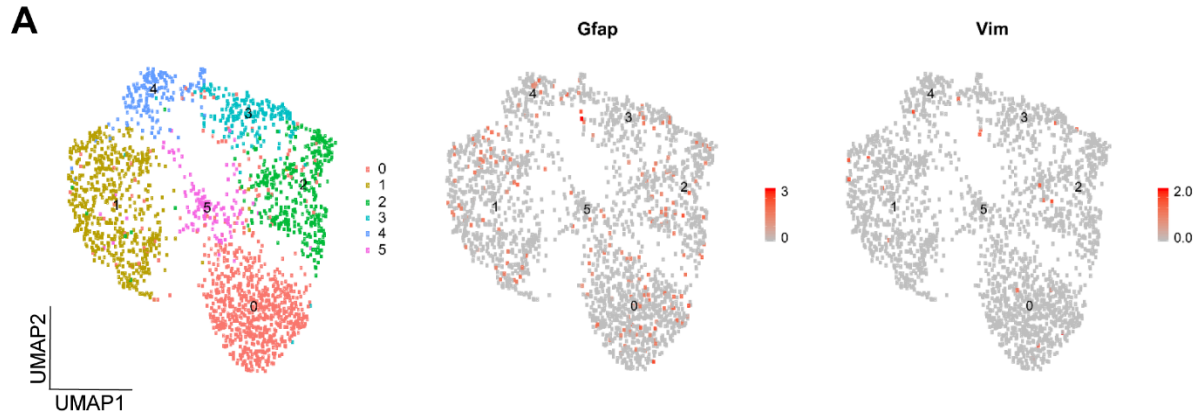
B



Supplementary Figure 1: Immunofluorescence showing that the Gq-DREADD is not expressed in neurons and microglia. (A) Representative fluorescence images of the hippocampus and cortex demonstrating Gq-DREADD virus spread (red; mCherry) and neurons (blue; NeuN). **(B)** Representative fluorescence images of the hippocampus and cortex demonstrating Gq-DREADD virus spread (red; mCherry) and microglia (blue; Iba1).



Supplementary Figure 2: Functional network of genes that are upregulated after Gq-DREADD activation in astrocytes. Processes that were enriched are G protein coupled receptor signaling pathway, ionotropic glutamate receptor signaling pathway, adenylate cyclase inhibiting G protein coupled receptor signaling pathway, cellular calcium ion homeostasis, and calcium ion homeostasis. The upregulated genes are marked with red circles.



Supplementary Figure 3: No major change in the expression of reactive astrogliosis markers. (A) UMAP of the astrocyte subclusters shows very low or no expression of markers for activated astrocytes.

Supplementary Tables

Supplementary Table 1: Percentage of cells present in the identified cell clusters.

Cluster	Saccharin (%)	CNO (%)	Cell Type
0	30.66	45.32	Mixed Glia I
1	29.62	14.87	Mixed Glia II
2	12.37	16.74	Microglia I
3	11.39	6.60	Microglia II
4	7.41	5.30	Astrocytes
5	2.15	2.82	Microglia III
6	2.01	2.79	Microglia IV
7	1.56	1.07	Endothelial I
8	0.43	1.64	Ependymal I
9	0.61	0.76	Microglia V
10	0.59	0.81	Neuron
11	0.46	0.43	Ependymal II
12	0.29	0.49	Endothelial II
13	0.29	0.14	Endothelial III
14	0.11	0.17	Endothelial IV

Supplementary Table 2: Percentage of cells present in the astrocyte sub-clusters.

Cluster	Saccharin (%)	CNO (%)
0	53.26	3.96
1	0.87	66.55
2	26.96	1.52
3	14.13	0.47
4	1.01	18.30
5	3.77	9.21

Supplementary Table 3: Percentage of cells present in the mixed glia I sub-clusters.

Cluster	Saccharin (%)	CNO (%)
0	64.05	53.32
1	27.92	30.50
2	0.78	10.06
3	0.37	2.95
4	3.71	0.04
5	1.01	2.05
6	2.04	0.08
7	0.12	1.00

Supplementary Table 4: Percentage of cells present in the mixed glia II sub-clusters.

Cluster	Saccharin (%)	CNO (%)
0	56.90	11.66
1	37.12	0.87
2	2.69	66.26
3	0.05	20.45
4	3.13	0.62
5	0.11	0.12

Supplementary Table 5: Percentage of cells present in the microglia II sub-clusters.

Cluster	Saccharin (%)	CNO (%)
0	48.74	2.25
1	0.52	54.18
2	26.48	0.28
3	21.40	0.38
4	0.33	35.59
5	1.80	5.63
6	0.71	1.69

Supplementary Table 6: Percentage of cells present in the microglia I sub-clusters.

Cluster	Saccharin (%)	CNO (%)
0	54.12	12.81
1	7.11	44.62
2	5.02	38.74
3	28.74	1.78
4	0.00	5.27
5	5.02	0.07
6	0.00	0.71

Supplementary Table 7: Percentage of cells present in the microglia III sub-clusters.

Cluster	Saccharin (%)	CNO (%)
0	56.08	8.95
1	19.11	35.81
2	3.97	36.24
3	18.11	16.38
4	2.73	2.62

Supplementary Table 8: Percentage of cells present in the microglia IV sub-clusters.

Cluster	Saccharin (%)	CNO (%)
0	14.67	45.09
1	0.80	48.66
2	50.40	0.00
3	22.67	0.00
4	11.47	6.25

Supplementary Table 9: Percentage of cells present in the microglia V sub-clusters.

Cluster	Saccharin (%)	CNO (%)
0	23.73	40.80
1	33.90	25.60
2	30.51	17.60
3	11.86	16.00

Supplementary Table 10: Percentage of cells present in the neuron sub-clusters.

Cluster	Saccharin (%)	CNO (%)
0	51.85	37.40
1	30.56	27.48
2	17.59	35.11